Following the relaxation dynamics of photoexcited aniline in the 273-266 nm region using time-resolved photoelectron imaging

Following the relaxation dynamics of photoexcited aniline in the 273-266 nm region using time-resolved photoelectron imaging

James O. F. Thompson, Ruth A. Livingstone, and Dave Townsend

Citation: The Journal of Chemical Physics **139**, 034316 (2013); doi: 10.1063/1.4813005
View online: http://dx.doi.org/10.1063/1.4813005
View Table of Contents: http://scitation.aip.org/content/aip/journal/jcp/139/3?ver=pdfcov
Published by the AIP Publishing

Following the relaxation dynamics of photoexcited aniline in the 273-266 nm region using time-resolved photoelectron imaging

James O. F. Thompson, Ruth A. Livingstone,[a] and Dave Townsend[b]
Institute of Photonics and Quantum Sciences, Heriot-Watt University, Edinburgh EH14 4AS, United Kingdom

(Received 24 May 2013; accepted 20 June 2013; published online 18 July 2013)

Time-resolved photoelectron imaging was used to investigate the relaxation dynamics of electronically excited aniline in the gas-phase following ultraviolet irradiation in the 273-266 nm region. We find that at all wavelengths studied, excitation is predominantly to the long-lived (>1 ns) $S_1(\pi\pi^*)$ state, which exhibits ultrafast intramolecular vibrational redistribution on a <1 ps timescale. At excitation wavelengths centred on resonant transitions in the aniline absorption spectrum that have previously been assigned to the higher lying $S_2(3s/\pi\sigma^*)$ state, we also see clear evidence of this state playing a role in the dynamics. However, we see no indication of any non-adiabatic coupling between the $S_1(\pi\pi^*)$ and $S_2(3s/\pi\sigma^*)$ states over the range of excitation wavelengths studied.
 [http://dx.doi.org/10.1063/1.4813005]

I. INTRODUCTION

In recent years, the excited state electronic relaxation dynamics operating in a wide range of simple aromatic systems has become the subject of considerable theoretical and experimental investigation.[1,2] This interest has been primarily motivated by the fact that such systems often form the chromophore sites for ultraviolet (UV) absorption in larger biological species (for example, the DNA bases, the melanin pigmentation system, various amino acids, and phenylpropanoids in plants).[3,4] There is growing evidence that non-adiabatic couplings between the electronic and vibrational degrees of freedom in these species may provide a rapid, efficient route for the dissipation of excess energy into the surrounding environment—greatly reducing the possibility of other, potentially more harmful photochemical processes taking place.[1,3] This imparts a critical photostability that may have provided an important evolutionary factor in the development of early life $\sim 3.5 \times 10^9$ yr ago. At that time, the surface of the Earth was subject to much more intense UV irradiation than today as the atmosphere was not yet fully developed.[5]

One example of a small aromatic system that has attracted a great deal of recent attention is aniline (aminobenzene), which provides an analogue model system approximating subunits in several biological species. Early spectroscopic studies of aniline identified two bright absorption bands in the UV region between 300 and 220 nm, which were assigned to transitions of $^1\pi\pi^*$ character.[6,7] More recent theoretical[8] and experimental[9] work has also identified an additional, weak transition that corresponds to excitation from the highest occupied π molecular orbital to the lower adiabat resulting from a strong coupling interaction between a bound 3*s* Rydberg state and a valence state of σ^* character that is purely repulsive along the N–H coordinate. A good schematic illustration of this interaction may be found in Fig. 7 of a recent publication by Ashfold and co-workers.[10] This state is energetically located between the two aforementioned $^1\pi\pi^*$ transitions, with an experimentally determined origin reported at 269.5 nm.[9] In the remainder of this paper, we will use $S_1(\pi\pi^*)$, $S_2(3s/\pi\sigma^*)$, and $S_3(\pi\pi^*)$ to denote the three lowest lying excited singlet electronic states of aniline. More generally, low-lying excited electronic states formed via Rydberg/valence interactions (often simply dubbed "$\pi\sigma^*$" states even though they are formally of mixed character) are now recognised as a common feature in the gas-phase excited state photochemistry of many molecular systems, including biologically relevant motifs such as phenols,[11–13] pyrroles,[14,15] imidazoles,[16–19] and indoles.[20–22] Excitation in the vertical Franck-Condon region primarily samples the 3*s* Rydberg character, however, upon extension along an X–H bond (where X may be N or O in the examples listed above), the Rydberg electron density evolves into an orbital of predominantly σ^* character. This may therefore give rise to direct bond fission and H atom elimination or, alternatively, may lead to non-adiabatic relaxation mechanisms proceeding via internal conversion through conical intersections (CIs) with other electronic states. Since this often includes the S_0 ground state, "$\pi\sigma^*$" states have been implicated in providing the aforementioned rapid and efficient "photoprotective" pathway employed by nature for the dissipation of excess electronic energy back into the surrounding environment. An in-depth discussion of the Rydberg/valence coupling interaction may be found in the recent review of Reisler and Krylov.[23] In contrast to many other molecules exhibiting such states, we highlight that in aniline the $S_2(3s/\pi\sigma^*)$ state exhibits a potential well along the N–H coordinate that is sufficiently deep to support a number of bound vibrational levels. This is primarily a consequence of its relatively low ionization potential leading to a reduction of the 3*s* Rydberg state energy relative to the $\pi\sigma^*$ valence state (when compared, for example, to the isoelectronic species phenol, in which the $S_2(3s/\pi\sigma^*)$ state does not support any bound vibrational levels).[11]

[a]Present address: Max Planck Institute for Polymer Research, Ackermannweg 10, 55128 Mainz, Germany.
[b]Author to whom correspondence should be addressed. Electronic mail: D.Townsend@hw.ac.uk

In recent years, the UV excitation dynamics of gas-phase aniline has been the subject of four independent studies reported by research groups employing a range of different experimental techniques and associated observables. This previous work serves as a basis for both the motivation and discussion of our present paper. In the first of these, Ashfold and co-workers used H Rydberg atom photofragment translational spectroscopy to investigate the excitation region spanning 293.9–193.3 nm.[10] At wavelengths longer than 269.5 nm, only a very broad, low-energy H atom loss feature was observed in the total kinetic energy release (TKER) spectra. This was attributed predominantly to multiphoton excitation (with subsequent fragmentation) that was resonantly enhanced via the $S_1(\pi\pi^*)$ state. These signals exhibited no significant recoil anisotropy, indicating a long dissociation lifetime relative to the period of molecular rotation. At wavelengths $\leq$269.5 nm (the location of the $S_2(3s/\pi\sigma^*)$ origin) additional very sharp H atom loss features were observed. These were assigned to the initial excitation of quasibound vibrational levels within the shallow potential well present along the N–H coordinate of the $S_2(3s/\pi\sigma^*)$ state in the Franck-Condon region. It was then proposed that fission of the N–H bond subsequently proceeds via H atom tunnelling under the shallow exit barrier encountered at more extended N–H distances. The H atom recoil anisotropy parameter of $\beta = -0.5$ associated with this pathway provided evidence of an extremely rapid process. As the excitation wavelength was shortened further (<260 nm), a broader, unstructured high TKER continuum began to appear in place of the sharp features. This was attributed to excitation to the $S_1(\pi\pi^*)$ state with subsequent internal conversion to $S_2(3s/\pi\sigma^*)$. At excitation below 230 nm, further changes in the H atom TKER spectra were taken as evidence for the onset of absorption to the higher lying $S_3(^1\pi\pi^*)$ state.

A second study by Longarte and co-workers employed time-resolved ion yield spectroscopy to investigate the 294–234 nm pump excitation region, with subsequent ionization using several different multiphoton probe schemes and polarization geometries.[24] At excitation energies below the $S_2(3s/\pi\sigma^*)$ origin, only a long-lived transient signal was observed. This was assigned to direct excitation exclusively to the $S_1(\pi\pi^*)$ state. Between 269.5 and 240 nm, a very weak, much more rapidly decaying signal was also seen (modelled with an exponential a time constant of 165 fs) and assigned to direct population of the $S_2(3s/\pi\sigma^*)$ state. At excitation wavelengths below 240 nm, additional decaying components appearing in the observed transient ion signals were attributed to the onset of $S_3(^1\pi\pi^*)$ excitation.

More recently, Stavros and co-workers investigated the H-atom elimination channel(s) in aniline using a time-resolved ion-imaging approach following excitation at selected wavelengths over the 294-200 nm range.[25] In contrast to the two previous studies discussed above, this work observed no evidence for direct excitation to the $S_2(3s/\pi\sigma^*)$ state at wavelengths >250 nm. This was attributed to the large bandwidth of the femtosecond pulses used in this study giving rise to inefficient population of the $S_2(3s/\pi\sigma^*)$ state (which exhibits comparatively narrow resonant features in this energy region) relative to the much stronger and broadly overlapping signals associated with the $S_1(\pi\pi^*)$ transition. However, at excitation wavelengths <250 nm this work did begin to see evidence of the $S_2(3s/\pi\sigma^*)$ state operating as a <1 ps non-adiabatic relaxation pathway for the initially populated $S_1(\pi\pi^*)$ state—in general agreement with the findings of the Ashfold group. At pump wavelengths $\leq$240 nm excitation to higher lying $^1\pi\pi^*$ states was also reported, with a subsequent two-stage, sequential decay pathway proceeding via both $S_1(\pi\pi^*)$ and $S_2(3s/\pi\sigma^*)$.

Finally, Fielding and co-workers used time-resolved photoelectron imaging (TRPEI) to follow the ultrafast dynamics of aniline following excitation in the 269-236 nm region.[26,27] The work concluded that at 269 nm, in addition to some direct excitation to the long-lived $S_1(\pi\pi^*)$ state, both the 3*s* Rydberg and $\pi\sigma^*$ components of the S_2 state were excited simultaneously. These two components were observed to exhibit 1/*e* lifetimes of 230 fs and 0.9 ps, respectively, with the former being attributed to decay via non-adiabatic coupling to $S_1(\pi\pi^*)$ and the latter to dissociation along the N–H coordinate on the initially prepared $\pi\sigma^*$ component. At 250 nm excitation was reported to proceed exclusively via the 3*s* and $\pi\sigma^*$ components, with no direct population of $S_1(\pi\pi^*)$. At pump wavelengths $\leq$240 nm the onset of excitation to $S_3(^1\pi\pi^*)$ was also observed.

There are some clear discrepancies that exist between the various dynamical studies described above—particularly following excitation close to the $S_2(3s/\pi\sigma^*)$ origin. In order to attempt to resolve this, we present a detailed study of this region employing the TRPEI technique at 4 different excitation wavelengths spanning 273-266 nm. More specifically, these wavelengths were centred at (i) 273 nm—which sits 3.5 nm to the red of the $S_2(3s/\pi\sigma^*)$ origin; (ii) 269.5 nm—the $S_2(3s/\pi\sigma^*)$ origin; (iii) 267.7 nm—a region sitting in between the first two resonant transitions assigned to the $S_2(3s/\pi\sigma^*)$ state; and (iv) 265.9 nm—a second, very broad resonant feature in $S_2(3s/\pi\sigma^*)$ absorption spectrum. For further details see Fig. 4 of Ref. 9. The highly differential energy- and angle-resolved data afforded by the TRPEI approach unambiguously reveal signatures of the $S_2(3s/\pi\sigma^*)$ state, however, we find no evidence that the $S_1(\pi\pi^*)$ and $S_2(3s/\pi\sigma^*)$ states undergo any interaction via non-adiabatic coupling over the range of excitation energies studied.

II. EXPERIMENTAL

The experimental set-up has been recently described in detail elsewhere.[28] Aniline (Sigma-Aldrich, 99%) was introduced into the source chamber of a differentially pumped photoelectron spectrometer via an Even-Lavie pulsed molecular beam valve operating at 1 kHz.[29] A small strip of filter paper was soaked with sample and placed in a cartridge mounted within the valve body, directly behind the exit nozzle. Helium at a pressure of 3 bar was used as a carrier gas and the valve temperature was regulated at 50 °C using a closed-loop chiller. After travelling through a skimmer, the molecular beam passed into the main interaction chamber and was intersected at 90° by co-propagating UV pump and probe pulses. Both pulses were produced from the fundamental output of a 1 kHz regeneratively amplified Ti:Sapphire laser

system (Spectra-Physics, Spitfire Pro/Empower) seeded by a Ti:Sapphire oscillator (Spectra Physics, Tsunami/Millennia Pro). The output bandwidth from the amplifier was set to ~25 nm and the central wavelength was tuned between 819 and 798 nm via the seed. The pump beam (273-266 nm, attenuated to ~0.2 μJ/pulse) was provided by the third harmonic of this output, generated using a pair of thin (0.1 mm) beta barium borate (BBO) crystals. Material dispersion compensation was achieved using a double-pass CaF_2 prism compressor. The probe beam (305 nm, ~0.5 μJ/pulse) was generated by twice frequency doubling the signal beam output from an optical parametric amplifier (Spectra Physics, OPA-800C) pumped by the Ti:Sapphire system. The probe wavelength was chosen to ensure that it would induce no absorption to the $S_1(\pi\pi^*)$ state, eliminating the possibility of any unwanted "probe-pump" dynamics appearing in the photoelectron spectra close to zero delay times. Dispersion management of this beam line was achieved using a double-pass fused silica prism compressor. The temporal delay between the pump and the probe was precisely controlled using a linear translation stage (Physik Instrumente, M-403.62S) and controller (Physik Instrumente, Mercury Step) running under PC control. The pump and probe beams were combined on a 2.0 mm dichroic mirror and focussed into the spectrometer though 2.0 mm CaF_2 window using a 25 cm fused silica lens.

The interaction between the UV light pulses and the molecular beam took place between the repeller and extractor electrodes of a mu-metal shielded electrostatic lens set-up optimised for velocity-map imaging of photoelectrons produced following (1+1′) ionization of aniline.[30] A 40 mm dual MCP/P47 phosphor screen detector (Photonis, APD 2 PS 40/12/10/12 I 46:1 P47) was positioned at the end of the photoelectron flight tube. The applied voltage on the back microchannel plate was gated using a high voltage pulser (DEI, PVX-4140). Photoelectrons impacting on the detector were imaged using a monochrome Firewire CCD camera (The Imaging Source, DMK 21BF04) with a 640 × 480 pixel array. Data were passed from the camera to a PC running acquisition software at 30 frames per second. No additional processing of the raw images was performed prior to the full analysis of the data.

By systematically adjusting the length of the prism compressor in each beam line, a pump-probe cross correlation of 180 ± 20 fs was obtained. This was recorded directly inside the spectrometer from non-resonant, two-colour (1 + 1′) multiphoton ionization of pyrrole. Time-of-flight to energy calibration of the instrument was obtained from two-photon, non-resonant ionization of 1,3-butadiene (at 250 nm) and the central wavelengths of both the pump and probe beams were accurately monitored using a universal serial bus (USB) grating spectrometer (Ocean Optics, USB2000+). Data collection runs consisted of scanning the translation stage repeatedly between pump-probe delays of −300 fs to +1000 fs in 33.3 fs increments and +1000 fs to +3600 fs in 200 fs increments (giving 53 time steps per data set in total). At each repeatedly sampled delay position, pump-probe photoelectron images were recorded for 5 s, along with images of the time-invariant one-colour pump alone and probe alone signals (for subsequent background subtraction). Typical data accumulation runs at each pump wavelength studied constituted approximately 30–40 scans in total. Photoelectron image data from all individual scans, recorded at each specific pump-probe delay, were then added together for subsequent processing and analysis. Given the very short-time dynamics that are observed in the data recorded at certain excitation wavelengths (*vida infra*), this analysis is potentially extremely sensitive to any small offsets or drifts in the position of zero pump-probe delay time. As such, data collection on each acquisition run was periodically suspended in order to check that no such issues were present.

III. RESULTS

A. Time-resolved photoelectron spectra

In Fig. 1, we present a series of photoelectron images resulting from (1 + 1′) ionization of aniline at a pump-probe delay time $\Delta t = 100$ fs following excitation at each of the four pump wavelengths studied. These data were generated by subtracting one-colour pump-alone and probe-alone background images from the raw pump-probe image. The right hand half of each image shows the result following application of a rapid matrix inversion approach that has been described in detail elsewhere.[28] Of particular note is the clearly visible, very sharp, and highly anisotropic outer ring in the data recorded at pump wavelengths of 269.5 nm and 265.9 nm. This ring is somewhat more intense in the latter case. Using appropriate time-of-flight to energy calibration information, time-resolved photoelectron spectra may be generated from the full

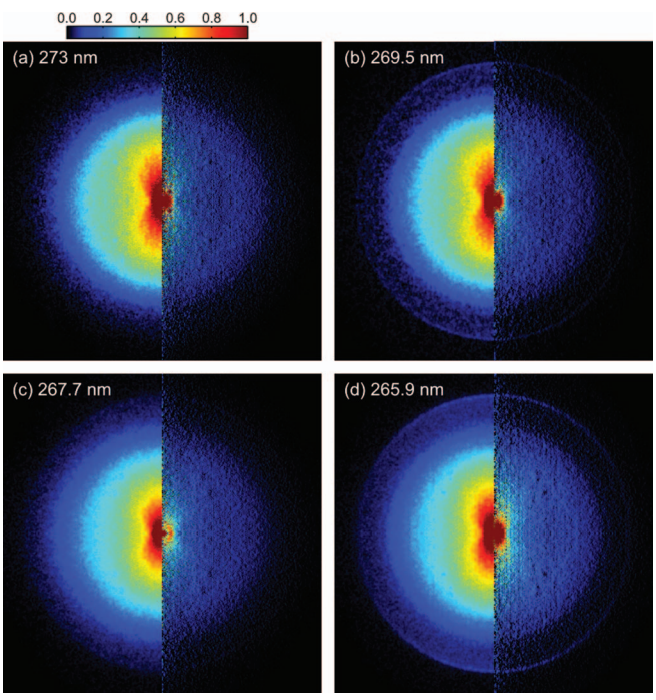

FIG. 1. (1+1′) photoelectron images recorded from aniline at pump-probe delay time $\Delta t = 100$ fs for the four different pump excitation wavelengths used in this study. Pump-alone and probe-alone signals have been subtracted and the images are 4-fold symmetrised. The linear polarization direction of both the pump and probe beams is vertical with respect to the images. The right half of the images show the processed data obtained following application of the matrix inversion method described in Ref. 28.

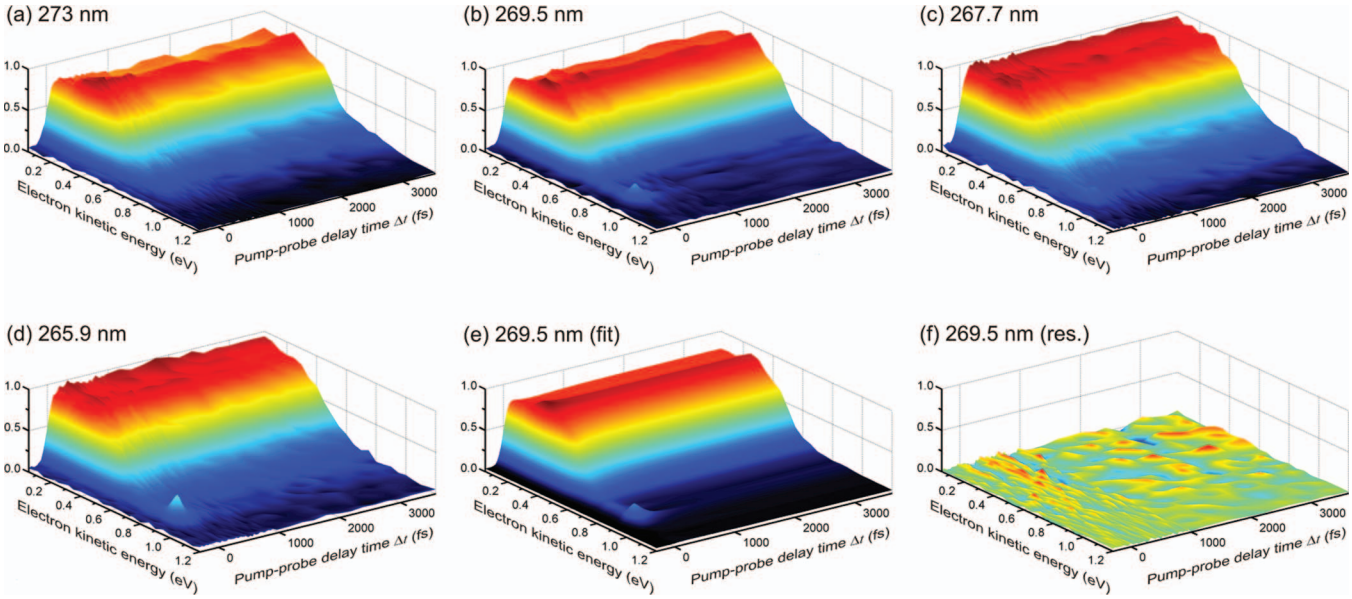

FIG. 2. Time-dependent photoelectron spectra of aniline obtained following excitation at four different pump excitation wavelengths with subsequent ionization using a 305 nm probe. The data are partitioned into 0.05 eV energy bins. Also shown are the fit to the 269.5 nm data obtained using the procedure described in the main text as well as the associated residuals (i.e., the fit subtracted from the raw data).

set of background-subtracted image data recorded at each of the four pump wavelengths used in the present study. These plots are shown in Figs. 2(a)–2(d). The data show no "probe-pump" dynamics evolving to negative time delays due to our choice of probe wavelength (305 nm). Within the small range of total photon (i.e., pump + probe) energies used in the experiments (~8.6-8.7 eV), only the D_0 (π^{-1}) electronic state of the cation is accessible in all cases.[31,32] The adiabatic ionization potential of aniline is 7.72 eV.[33] The data recorded at 273 nm and 267.7 nm (Figs. 2(a) and 2(c)) appear to predominantly show only a long-lived feature spanning the 0.0–0.6 eV region, although there is a weakly decaying signal superimposed on top of this. In contrast, the data recorded at 269.5 nm and 265.9 nm (Figs. 2(b) and 2(d)) show an additional narrow, very rapidly decaying feature between 0.9 and 1.0 eV, with this signal being more pronounced in the shorter wavelength instance.

The time dependence of the photoelectron data was analysed using a standard Levenberg-Marquardt global fitting routine wherein the 2D data $S(E, \Delta t)$ are expressed as[34]

$$S(E, \Delta t) = \sum_i A_i(E) \cdot P_i(\Delta t) \otimes g(\Delta t). \qquad (1)$$

Here, $A_i(E)$ is the decay associated photoelectron spectrum of the ith data channel, which has a time-dependent population $P_i(\Delta t)$ described by a series of exponentially decaying functions (all of which originate from zero pump-probe delay) and $g(\Delta t)$ is the experimentally determined Gaussian cross-correlation function. This approach yields a series of decay associated spectra (DAS) that plot the relative amplitude of each exponential component as a function of electron kinetic energy. Additional information on this approach may be found elsewhere.[34]

In order to non-trivially fit the 273 nm data set shown in Fig. 2(a) using Eq. (1), just two exponential functions were required. One of these exhibits a time constant $\tau_2 = 640$ fs and the other, assigned as τ_3, is very long-lived (>1 ns). Fig. 3(a) shows the DAS plots along with the associated time constants (which have an associated uncertainty of ±10%). In this case, the excitation wavelength (273 nm) was centred on an absorption region where no significant direct excitation to a resonant feature of the $S_2(3s/\pi\sigma^*)$ spectrum is expected since

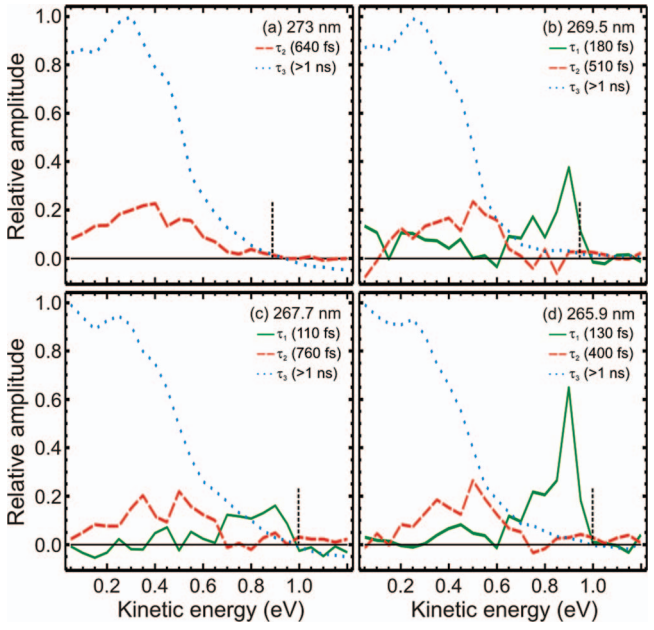

FIG. 3. Decay associated spectra obtained from a global exponential fit to the data presented in Figs. 2(a)–2(d). For additional details see the main text. The uncertainty in the values of all quoted time constants is ±10%. The vertical dashed line on the energy axis denotes the maximum predicted photoelectron kinetic energy resulting from (1+1′) ionization taking the central wavelengths of the pump and probe pulses and the adiabatic ionization potential of 7.72 eV previously reported in Ref. 33. The data are partitioned into 0.05 eV energy bins.

we are sitting ~475 cm^{-1} below the origin. In the case of the data shown in Figs. 2(b) and 2(d), where the pump excitation was centred on a transition resonant with the $S_2(3s/\pi\sigma^*)$ state, the inclusion of a third exponentially decaying function, exhibiting a much shorter lifetime, was clearly required to produce a satisfactory global fit. The corresponding DAS are presented in Figs. 3(b) and 3(d). To illustrate the good quality of the overall fitting model, Figs. 2(e) and 2(f) show the corresponding fit and associated residuals for the 269.5 nm data. At the $S_2(3s/\pi\sigma^*)$ origin (269.5 nm), our value of $\tau_1 = 180$ fs is in good agreement with the short-decay lifetimes previously reported by Longarte and co-workers[24] (165 fs) and Fielding and co-workers[27] (230 fs). At 267.7 nm (exciting between the first two resonant features in the $S_2(3s/\pi\sigma^*)$ absorption spectrum), it was found that a two-exponential fit gave rise to a small but non-zero amplitude in the region spanning 0.9–1.0 eV. This is a consequence of a small amount of excitation to resonant $S_2(3s/\pi\sigma^*)$ transitions induced by the wings of the broadband pump laser pulse. As such, the τ_2 lifetime appeared skewed to a shorter value and so a three-exponential fit was deemed appropriate. This is shown in Fig. 3(c) where the DAS plot for the short lived τ_1 component we have included exhibits only very weak amplitude in the 0.9–1.0 eV region compared to the data recorded at 269.5 nm and 265.9 nm. We also highlight the fact that the relative shapes and amplitudes for the τ_2 and τ_3 DAS are very similar at all four excitation wavelengths and note that for all data sets, the limited range of pump-probe delay times sampled in the experiments means we are only able to place a lower limit of >1 ns on τ_3. This lower limit was confirmed by performing additional exploratory scans out to pump-probe delay times of 100 ps.

Although the time constants for the three DAS plots at 269.5 nm excitation (as shown in Fig. 3(b)) appear to be in good agreement with the previously reported TRPEI work of Fielding and co-workers,[27] the relative amplitude associated with the shortest time constant is somewhat different: In our data no significant negative amplitude component is observed in any kinetic energy region, whereas the former study observed the DAS that we have assigned as τ_1 to be strongly negative between 0.0 and 0.6 eV. We note, however, that this work employed a different method to extract the DAS than the global fitting approach used here. The absence of any negative features in our τ_1 DAS would seem to be consistent with several other aspects of our data, as discussed later.

B. Photoelectron angular distributions

For the case of a two-photon ionization scheme using linear polarization, the time-dependent photoelectron angular distributions (PADs) we have obtained may be expressed as a function of the electron kinetic energy E and the pump-probe delay time Δt in terms of the well-known anisotropy parameters β_2 and β_4:[35,36]

$$I(E, \Delta t, \theta) = \frac{\sigma(E, \Delta t)}{4\pi}[1 + \beta_2(E, \Delta t)P_2(\cos\theta) + \beta_4(E, \Delta t)P_4(\cos\theta)]. \quad (2)$$

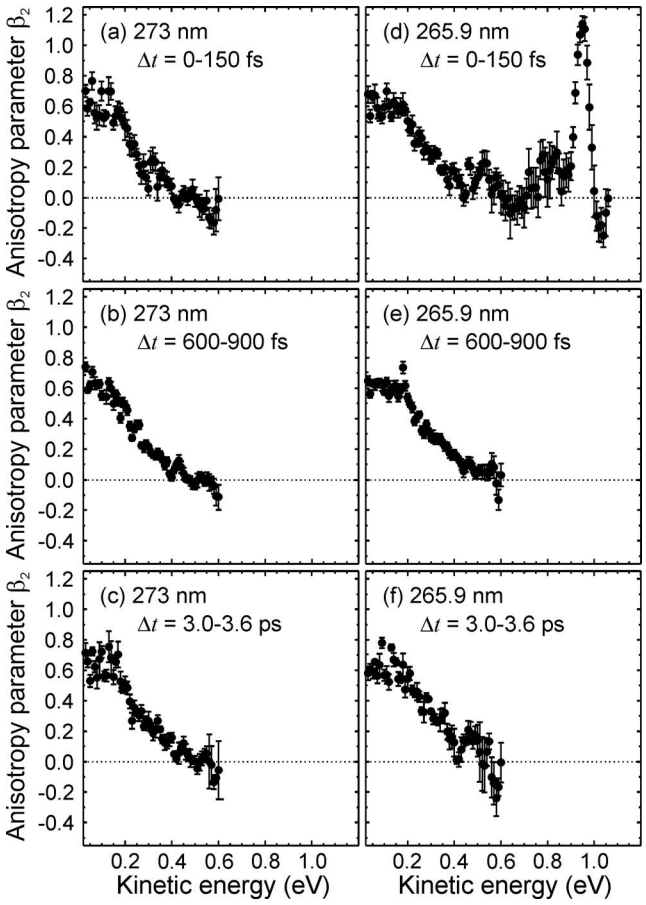

FIG. 4. Anisotropy parameter β_2 as a function of photoelectron kinetic energy averaged over a selected range of pump-probe delay times, Δt, following aniline excitation at 273 nm and 265.9 nm (with subsequent ionization using 305 nm). The fits were performed over the angular region between $5^\circ \le \theta \le 90^\circ$ to eliminate uncertainties from the centre-line noise present in the Abel-inverted images and the data are partitioned into 0.01 eV energy bins. The error bars represent one standard deviation. With the exception of (d), the plots are truncated at 0.6 eV as beyond this point the signal level in the raw photoelectron data is so small that the fit becomes statistically meaningless.

Here the $P_n(\cos\theta)$ terms are the nth-order Legendre polynomials, $\sigma(E, \Delta t)$ is the time-dependent electron energy distribution, and $\theta = 180^\circ$ is defined by a vertical line running fully through the images shown in Fig. 1 via the centre point. Performing a fit to our data using Eq. (2) reveals that, within statistical uncertainty, β_4 is effectively zero over all regions of the time-dependent photoelectron spectra recorded for all molecules under study. However, the PADs do exhibit significant overall anisotropy which is strongly energy dependent. This is quantified in Fig. 4, which plots β_2 as a function of photoelectron kinetic energy averaged over three different pump-probe delay regions following excitation at 273 nm and 265.9 nm. Of particular note is that (i) the region between 0.9 and 1.0 eV in the 265.9 nm data averaged between 0 and 150 fs (see Fig. 4(d)) exhibits a relatively high degree of anisotropy ($\beta_2 \sim 1.1$) and (ii) at both excitation wavelengths the shape of the anisotropy plots between 0.0 and 0.6 eV is extremely similar for all pump-probe delay regions sampled. Additionally, the data appear to exhibit no significant temporal evolution. This observation is further reinforced in Fig. 5

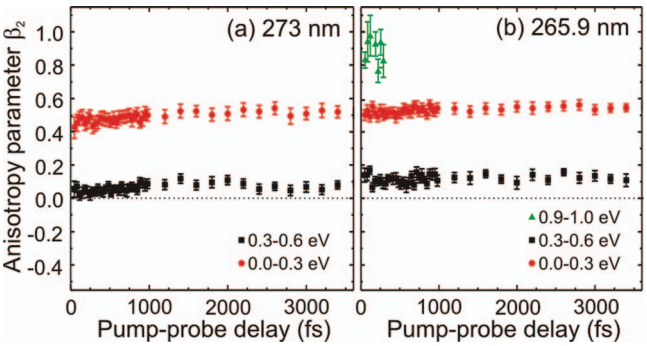

FIG. 5. Anisotropy parameter β_2 as a function of pump-probe delay time averaged over a selected range of photoelectron kinetic energies following aniline excitation at 273 nm and 265.9 nm (with subsequent ionization using 305 nm). As with the data shown in Fig. 4, the fits were performed over the angular region between $5^\circ \leq \theta \leq 90^\circ$ to eliminate uncertainties from the centre-line noise present in the Abel-inverted images and the data for the fit were partitioned into 0.01 eV energy bins. The error bars represent one standard deviation. In (b) the 0.9–1.0 eV plot is truncated at 300 fs and beyond as the signal level in the raw photoelectron data becomes so small that the fit becomes statistically meaningless.

which presents β_2 plotted over the full range of pump-probe delays used in our measurements for three different kinetic energy regions. Finally, it should also be pointed out that the data recorded at 267.7 nm and 269.5 nm show near identical behaviour to that presented for 273 nm and 265.9 nm, respectively.

IV. DISCUSSION

A. The role of the $S_1(\pi\pi^*)$ state

On the basis of previous spectroscopic studies, it is known that excitation at 273 nm is expected to only populate the $S_1(\pi\pi^*)$ state of aniline.[9,10] In addition, the lifetime of the $S_1(\pi\pi^*)$ state at this excitation energy is known to be very long lived (~6 ns).[37] It is therefore reasonable to assign the $\tau_3 > 1$ ns decay constant we obtain from our global fit at this wavelength to $S_1(\pi\pi^*)$. The ultimate fate of the $S_1(\pi\pi^*)$ state is not apparent in our data but we note that, in addition to decay via fluorescence, previous work by Weber and co-workers reported the rise of a long-lived (ns) component in a picosecond time-resolved photoelectron spectroscopy measurement following aniline excitation at 294 nm (the $S_1(\pi\pi^*)$ origin[38]) and subsequent ionization using a 200 nm probe.[39] This signal, observed at ionization energies in excess of 9 eV, was assigned to relaxation via intersystem crossing to the T_1 triplet state. Our current measurements (which have a maximum pump + probe energy of 8.7 eV) are therefore effectively "blind" to this pathway. We also note that Ashfold and co-workers have speculated that $S_1(\pi\pi^*)$ decay via internal conversion through a conical intersection with the S_0 state is likely to be inefficient at excitation wavelengths >260 nm.[10]

We now consider the origin of the decaying component in the 273 nm data characterised by $\tau_2 = 640$ fs. In previous work we have observed similar dynamical timescales in the $S_1(\pi\pi^*)$ states of phenol, catechol, resorcinol, and hydroquinone.[28] This was attributed to ultrafast intramolecular vibrational redistribution (IVR) leading to a change in the Franck-Condon factors for ionization which manifests itself as a temporal evolution of the ionization cross-section. We also note that ultrafast (i.e., sub-picosecond) IVR processes have been previously reported in the $S_1(\pi\pi^*)$ state of chlorobenzene[40] and the ground state of benzene and the difluorobenzenes.[41] In the experiments under discussion here, we are sitting ~2600–3580 cm^{-1} above the $S_1(\pi\pi^*)$ origin. This is also well above the experimentally determined IVR onset threshold in the excited $^1\pi\pi^*$ states of similar aromatic systems such as hydroquinone (1650 cm^{-1}) and anisole (940 cm^{-1}).[42,43] On the basis of this evidence, we therefore attribute the τ_2 signal in our 273 nm data to an ultrafast IVR process. The aforementioned work of Longarte and co-workers has also speculated that such a process may be taking place on the initially prepared $S_1(\pi\pi^*)$ surface to account for this state exhibiting a relatively long lifetime even at excitation wavelengths as short as 240 nm.[24]

When compared with the data recorded at 273 nm, the data recorded at excitation wavelengths between 269.5 and 265.9 nm all clearly exhibit very similar timescales and relative amplitudes for the DAS relating to the decay channels described by τ_2 and τ_3—as seen in Figs. 3(b)–3(d). It therefore seems entirely reasonable to assume that at all excitation wavelengths used in this present study, an identical mechanism is in operation—i.e., a direct excitation to the $S_1(\pi\pi^*)$ state with subsequent IVR leading to an evolution in the total cross-section for ionization on a <1 ps timescale. We note that a possible alternative explanation for the τ_2 DAS signal is that of decay via "prefulvenic" conical intersections with the S_0 state—especially given that Fielding and co-workers have previously attributed sub-picosecond dynamical signatures to such pathways following UV excitation in the "channel 3 region" of benzene.[44,45] However, complete active space self-consistent field (CASSCF) calculations by Stavros and co-workers predict the energetic onset for non-adiabatic decay via prefulvenic CIs connecting the $S_1(\pi\pi^*)$ and S_0 states in aniline to lie ~5.50-5.61 eV above the S_0 minimum.[25] In addition to this threshold lying well above the range of pump energies used in our present study (4.54-4.66 eV), we note that these authors also inferred no strong evidence of the prefulvenic pathway in their experimental measurements at excitation wavelengths even as short as 200 nm—instead attributing their observed onset of sub-picosecond H atom elimination timescales at excitation wavelengths <250 nm to a CI between the $S_1(\pi\pi^*)$ and $S_2(3s/\pi\sigma^*)$ states.

B. The role of the $S_2(3s/\pi\sigma^*)$ state

Central pump wavelengths of 269.5 nm and 265.9 nm correspond to resonant excitation to bound vibrational levels within the $S_2(3s/\pi\sigma^*)$ state.[9] In both of these instances our data exhibit an additional, very rapidly decaying component at photoelectron kinetic energies between 0.9 and 1.0 eV—as readily seen in Figs. 2 and 3. As already discussed in the Introduction, in the Franck-Condon region the $S_2(3s/\pi\sigma^*)$ state exhibits significant 3*s* Rydberg character. The additional feature in the 269.5 nm and 265.9 nm data is therefore fully consistent with excitation to this state since (i) we are exciting to a single

quasibound vibrational level within the shallow potential well along the N–H stretching coordinate of the $S_2(3s/\pi\sigma^*)$ state. Given the large amount of Rydberg character in the Franck-Condon region, a strong propensity for $\Delta v = 0$ ionization is therefore expected, giving rise to a very narrow peak in the photoelectron spectrum that should be essentially energy invariant with excitation wavelength—as is observed (see the τ_1 DAS plots in Figs. 3(b) and 3(d)); (ii) single-photon ionization from an orbital possessing significant 3*s* character should (at a first "atomic" level of approximation) give rise to photoelectron partial waves of exclusively *p* character, peaking strongly along the direction of laser polarization. As seen in Fig. 4, the anisotropy of the PADs in the 0.9–1.0 eV region ($\beta_2 \sim 1.1$) is therefore strongly characteristic of such a process. We also note that the signal attributed to $S_2(3s/\pi\sigma^*)$ excitation is more intense and exhibits a shorter lifetime in our 265.9 nm data compared to that seen at 269.5 nm. This is fully consistent with the spectral features previously reported by Ebata and co-workers[9] who observed the $S_2(3s/\pi\sigma^*)$ origin transition to exhibit a significantly narrower linewidth ($\sim$35 cm^{-1} full-width at half-maximum, FWHM) than the higher lying resonant feature at 265.9 nm ($\sim$150 cm^{-1} FWHM). The broader feature is strongly indicative of a shorter excited state lifetime and also means that a greater proportion of our pump bandwidth is effectively resonant with the $S_2(3s/\pi\sigma^*)$ transition in this instance—enhancing its appearance in our data relative to the $S_1(\pi\pi^*)$ signal. The FWHM linewidths quoted above are estimated from Fig. 4 of Ref. 9 and correspond to 1/*e* lifetimes of $\sim$150 fs and $\sim$35 fs, respectively. In the former case, this is in good agreement with τ_1 extracted from our data (180 fs). In the latter instance, the lifetime is presumably far too short to accurately resolve given our experimental instrument response function; however, our data ($\tau_1 = 130$ fs) clearly reveal the expected trend. As discussed previously, the time-resolved H-atom elimination experiments of Stavros and co-workers did not report any evidence of direct population of the $S_2(3s/\pi\sigma^*)$ state following excitation at the origin (269.5 nm). However, this is presumably due to the fact that – as pointed out by the authors themselves – this study reported a UV pump laser bandwidth of $\sim$500 cm^{-1} FWHM. This is significantly larger than that used in our present study ($\sim$300 cm^{-1} FWHM).

We now consider the dynamical fate of the $S_2(3s/\pi\sigma^*)$ state. Ashfold and co-workers have suggested that population of bound vibrational levels within the shallow potential well present along the N–H coordinate of the $S_2(3s/\pi\sigma^*)$ surface (i.e., at wavelengths >260 nm) leads to initial decay via a tunnelling mechanism rather than undergoing internal conversion to $S_1(\pi\pi^*)$.[10] Within this proposed mechanism, once the H atom is on the other side of this barrier (at more extended N–H distances where the repulsive $\pi\sigma^*$ component of the $S_2(3s/\pi\sigma^*)$ potential becomes significant) a rapid and direct dissociation then subsequently ensues. In addition to the short τ_1 lifetime that would be required to give rise to the previously observed anisotropic recoil of the dissociating H atoms,[10] our data would also appear to be consistent with this scheme in several other regards: First, the absence of any negative features in the τ_1 DAS plots shown in Figs. 3(b) and 3(d) would seem to indicate strongly that no relaxation takes place via the $S_1(\pi\pi^*)$ state—*i.e., the population and subsequent decay of the* $S_1(\pi\pi^*)$ *and* $S_2(3s/\pi\sigma^*)$ *states are two independent processes over the range of excitation wavelengths investigated*. This assertion is also supported by the experimentally determined onset threshold for internal conversion via the $S_2(3s/\pi\sigma^*)/S_1(\pi\pi^*)$ CI reported by Ashfold and co-workers[10] (<260 nm) and Stavros and co-workers[25] (<250 nm). In general, we note that the absence of such DAS negative signals does not *de facto* imply non-sequential (or independent) dynamics, however, in this particular instance the photoelectron signal attributable to the $S_2(3s/\pi\sigma^*)$ state appears fully spectrally resolved from that arising from $S_1(\pi\pi^*)$. As such, some negative signals in the τ_1 DAS between 0.0 and 0.6 eV would reasonably be expected in the case of any $S_2(3s/\pi\sigma^*)/S_1(\pi\pi^*)$ internal conversion.[46] Second, additional weight is added to the argument for independent population and subsequent decay pathways for the $S_1(\pi\pi^*)$ and $S_2(3s/\pi\sigma^*)$ states by the fact that no temporal evolution of the β_2 anisotropy parameter is observed in any region of our observed photoelectron spectra (see Figs. 4 and 5). As argued previously by ourselves[28] and others,[47,48] changes in PAD anisotropy with pump-probe delay provide a strong signature of the dynamical evolution of the electronic character of the state (or states) from which ionization is occurring. In the case of many aromatic and heteroaromatic systems, the coupling between states of $\pi\pi^*$ or $n\pi^*$ character with those of $\pi\sigma^*$ character must often be mediated by vibronic interactions, owing to pure electronic symmetry restrictions.[2] Such interactions typically require a distortion of the molecular framework (commonly involving some twisting or puckering motion of the ring system) to induce this coupling—which may subsequently facilitate non-adiabatic dynamical evolution of the initially excited system. Critically, the timescale for such motions and the associated changes in electronic character they induce should generally be resolvable in "ultrafast" experimental measurements such as the one described in this present study. Our recently reported work on phenol and the dihydroxybenzenes provides a particularly salient example of this, where the temporal evolution of β_2 was taken as strong evidence of geometry-dependent coupling between the $S_1(\pi\pi^*)$ and $S_2(3s/\pi\sigma^*)$ states present in these systems.[28] In this general regard, aniline is no exception here since the $S_1(\pi\pi^*)$ and $S_2(3s/\pi\sigma^*)$ states are of B_2 and B_1 electronic symmetry, respectively, within the C_{2v} point group (which is applicable given the predicted planar geometries).[8] Vibrational modes of a_2 symmetry are therefore required to induce any $S_1(\pi\pi^*)/S_2(3s/\pi\sigma^*)$ vibronic coupling. Although it presently remains unclear exactly which specific modes may be responsible, we note that out-of-plane distortions of the ring system have been suggested as the possible mediator for this interaction.[10,25] As already discussed, relaxation via $S_1(\pi\pi^*) \rightarrow S_2(3s/\pi\sigma^*)$ internal conversion in aniline has been strongly inferred at higher excitation energies. However, the absence of any temporal evolution of the β_2 anisotropy parameter with pump-probe delay in our data suggests that, at the range of excitation energies studied, any vibrational motion on the initially excited $S_2(3s/\pi\sigma^*)$ surface is unable to sample the relevant coordinate space required to induce coupling with $S_1(\pi\pi^*)$ and open up a potential

non-adiabatic decay pathway through the associated CI. Given that the $S_2(3s/\pi\sigma^*)$ decay therefore seems to be proceeding via tunnelling under the barrier along the N–H coordinate of the potential surface, in principle, one might expect the significant change in the orbital character on either side of this barrier ($3s$ to $\pi\sigma^*$) to be observable in the time evolution of the PADs in the 0.9–1.0 eV region. However, such a signature would be very short-lived given that the dissociation to form H atom products will then be extremely rapid once the barrier has been traversed. In addition, the fact that the molecular geometry is extremely extended at this point most likely means that our experiment is effectively blind to this orbital evolution on the basis of strongly unfavourable Franck-Condon factors for ionization, given our relatively low-energy 305 nm probe.

Finally, given that we have no information on the relative ionization cross sections for the $S_1(\pi\pi^*)$ and $S_2(3s/\pi\sigma^*)$ states, we are unable to quantify the fractional contribution of these two independent decay pathways to the "overall" dynamics. However, in many respects this is a meaningless comparison in this instance as we are comparing a broad, effectively "continuum-like" transition to $S_1(\pi\pi^*)$ with a relatively narrow resonant feature associated with excitation to $S_2(3s/\pi\sigma^*)$. As such, the contribution of each component is largely dependent on laser bandwidth.

V. CONCLUSION

Time-resolved photoelectron imaging has been used to investigate the electronic relaxation dynamics of the aniline molecule in the gas-phase following excitation in the 273-266 nm region. We conclude that at all wavelengths studied, the $S_1(\pi\pi^*)$ state is populated directly and undergoes ultrafast IVR on a sub-picosecond timescale. In addition, at excitation wavelengths centred on previously reported spectral features associated with direct excitation to the $S_2(3s/\pi\sigma^*)$ state, we also see clear evidence of a new channel participating in the relaxation dynamics—as indicated by a distinctive narrow spectral signature and a high degree of PAD anisotropy. However, within the limited range of excitation wavelengths studied, we see no evidence of any non-adiabatic coupling between the $S_1(\pi\pi^*)$ and $S_2(3s/\pi\sigma^*)$ states. This assertion is supported by three different aspects of our data: (i) The overall similarity of the raw photoelectron spectra and the relative shapes/amplitudes of the fitted τ_2 and τ_3 DAS in the 0.0–0.6 eV region at all excitation wavelengths studied (i.e., both above and below the $S_2(3s/\pi\sigma^*)$ origin); (ii) the fact that no negative amplitude features are seen in the 0.0–0.6 eV region of the τ_1 DAS recorded at excitation wavelengths where the $S_2(3s/\pi\sigma^*)$ state is directly populated; and (iii) no temporal evolution of the PADs is observed in any region of the photoelectron spectra recorded at any of the four excitation wavelengths investigated.

Overall, the analysis of our data appears to lead to conclusions that are largely consistent with the majority of other recent reports investigating the relaxation dynamics of electronically excited aniline in this UV absorption region,[10,24,25] although our findings are somewhat different to a previous TRPEI study.[27] Finally, we note that extending our TRPEI studies of aniline to shorter excitation wavelengths is of great interest. However, we have a strong desire, whenever possible, to work in a regime where our photoelectron data are (i) free from probe-pump dynamics evolving to negative time delays and (ii) are also not potentially convoluted by the use of multiphoton ionization probes (i.e., the data should be as "clean" as possible). Given this rationale, a current lack of fully tuneable UV output for both the pump and probe beams in our experimental set-up means that we have not pursued such a study at this time.

ACKNOWLEDGMENTS

This work was made possible by financial support from Engineering and Physical Sciences Research Council (EPSRC) Grant No. EP/G041717/1. J.O.F.T. and R.A.L. thank Heriot-Watt University for PhD funding. We also thank H. H. Fielding, V. G. Stavros, and G. M. Roberts for helpful comments and discussion.

[1] A. L. Sobolewski, W. Domcke, C. Dedonder-Lardeux, and C. Jouvet, Phys. Chem. Chem. Phys. **4**, 1093 (2002).
[2] M. N. R. Ashfold, G. A. King, D. Murdock, M. G. D. Nix, T. A. A. Oliver, and A. G. Sage, Phys. Chem. Chem. Phys. **12**, 1218 (2010).
[3] C. E. Crespo-Hernández, B. Cohen, P. M. Hare, and B. Kohler, Chem. Rev. **104**, 1977 (2004).
[4] C. S. Cockell and J. Knowland, Biol. Rev. **74**, 311 (1999).
[5] I. Cnossen, J. Sanz-Forcada, F. Favata, O. Witasse, T. Zegers, and N. F. Arnold, J. Geophys. Res. **112**, E02008, doi:10.1029/2006JE002784 (2007).
[6] K. Kimura, H. Tsubomura, and S. Nagakura, Bull. Chem. Soc. Jpn. **37**, 1336 (1964).
[7] K. Kimura and S. Nagakura, Mol. Phys. **9**, 117 (1965).
[8] Y. Honda, M. Hada, M. Ehara, and H. Nakatsuji, J. Chem. Phys. **117**, 2045 (2002).
[9] T. Ebata, C. Minejima, and N. Mikami, J. Phys. Chem. A **106**, 11070 (2002).
[10] G. A. King, T. A. A. Oliver, and M. N. R. Ashfold, J. Chem. Phys. **132**, 214307 (2010).
[11] R. N. Dixon, T. A. A. Oliver, and M. N. R. Ashfold, J. Chem. Phys. **134**, 194303 (2011).
[12] G. M. Roberts, A. S. Chatterley, J. D. Young, and V. G. Stavros, J. Phys. Chem. Lett. **3**, 348 (2012).
[13] A. S. Chatterley, J. D. Young, D. Townsend, J. M. Zurek, M. J. Paterson, G. M. Roberts, and V. G. Stavros, Phys. Chem. Chem. Phys. **15**, 6879 (2013).
[14] B. Cronin, M. G. D. Nix, R. H. Qadiri, and M. N. R. Ashfold, Phys. Chem. Chem. Phys. **6**, 5031 (2004).
[15] R. Montero, A. P. Conde, V. Ovejas, M. Fernandez-Fernandez, F. Castaño, J. R. V. de Aldana, and A. Longarte, J. Chem. Phys. **137**, 064317 (2012).
[16] A. L. Devine, B. Cronin, M. G. D. Nix, and M. N. R. Ashfold, J. Chem. Phys. **125**, 184302 (2006).
[17] D. J. Hadden, K. L. Wells, G. M. Roberts, L. T. Bergendahl, M. J. Paterson, and V. G. Stavros, Phys. Chem. Chem. Phys. **13**, 10342 (2011).
[18] R. Crespo-Otero, M. Barbatti, H. Yu, N. L. Evans, and S. Ullrich, Chem. Phys. Chem. **12**, 3365 (2011).
[19] R. Montero, A. P. Conde, V. Ovejas, M. Fernandez-Fernandez, F. Castaño, and A. Longarte, J. Phys. Chem. A **116**, 10752 (2012).
[20] R. Livingstone, O. Schalk, A. E. Boguslavskiy, G. Wu, L. T. Bergendahl, A. Stolow, M. J. Paterson, and D. Townsend, J. Chem. Phys. **135**, 194307 (2011).
[21] R. Montero, A. P. Conde, V. Ovejas, F. Castaño, and A. Longarte, J. Phys. Chem. A **116**, 2698 (2012).
[22] T. A. A. Oliver, G. A. King, and M. N. R. Ashfold, Phys. Chem. Chem. Phys. **13**, 14646 (2011).
[23] H. Reisler and A. I. Krylov, Int. Rev. Phys. Chem. **28**, 267 (2009).
[24] R. Montero, A. Peralta-Conde, V. Ovejas, R. Martínez, F. Castaño, and A. Longarte, J. Chem. Phys. **135**, 054308 (2011).
[25] G. M. Roberts, C. A. Williams, J. D. Young, S. Ullrich, M. J. Paterson, and V. G. Stavros, J. Am. Chem. Soc. **134**, 12578 (2012).

[26]R. Spesyvtsev, O. M. Kirkby, M. Vacher, and H. H. Fielding, Phys. Chem. Chem. Phys. **14**, 9942 (2012).
[27]R. Spesyvtsev, O. M. Kirkby, and H. H. Fielding, Faraday Discuss. **157**, 165 (2012).
[28]R. A. Livingstone, J. O. F. Thompson, M. Iljina, R. J. Donaldson, B. J. Sussman, M. J. Paterson, and D. Townsend, J. Chem. Phys. **137**, 184304 (2012).
[29]U. Even, J. Jortner, D. Noy, N. Lavie, and C. Cossart-Magos, J. Chem. Phys. **112**, 8068 (2000).
[30]A. T. J. B. Eppink and D. H. Parker, Rev. Sci. Instrum. **68**, 3477 (1997).
[31]T. Kobayashi and S. Nagakura, Bull. Chem. Soc. Jpn. **47**, 2563 (1974).
[32]J. P. Maier and D. W. Turner, J. Chem. Soc., Faraday Trans. 2 **69**, 521 (1973).
[33]M. A. Smith, J. W. Hager, and S. C. Wallace, J. Chem. Phys. **80**, 3097 (1984).
[34]O. Schalk, A. E. Boguslavskiy, and A. Stolow, J. Phys. Chem. A **114**, 4058 (2010).
[35]K. L. Reid, Annu. Rev. Phys. Chem. **54**, 397 (2003).
[36]T. Suzuki, Annu. Rev. Phys. Chem. **57**, 555 (2006).
[37]R. Scheps, D. Florida, and S. A. Rice, J. Chem. Phys. **61**, 1730 (1974).
[38]J.-H. Yeh, T.-L. Shen, D. G. Nocera, G. E. Leroi, I. Suzuka, H. Ozawa, and Y. Namuta, J. Phys. Chem. **100**, 4385 (1996).
[39]B. Kim, C. P. Schick, and P. M. Weber, J. Chem. Phys. **103**, 6903 (1995).
[40]Y.-Z. Liu, C.-C. Qin, S. Zhang, Y.-M. Wang, and B. Zhang, Acta Phys.-Chim. Sin. **27**, 965 (2011).
[41]R. S. von Benten, Y. Liu, and B. Abel, J. Chem. Phys. **133**, 134306 (2010).
[42]G. N. Patwari, S. Doraiswamy, and S. Wategaonkar, J. Phys. Chem. A **104**, 8466 (2000).
[43]R. Matsumoto, K. Sakeda, Y. Matsushita, T. Suzuki, and T. Ichimura, J. Mol. Struct. **735–736**, 153 (2005).
[44]D. S. N. Parker, R. S. Minns, T. J. Penfold, G. A. Worth, and H. H. Fielding, Chem. Phys. Lett. **469**, 43 (2009).
[45]R. S. Minns, D. S. N. Parker, T. J. Penfold, G. A. Worth, and H. H. Fielding, Phys. Chem. Chem. Phys. **12**, 15607 (2010).
[46]Since all exponentials used in the fit originate from $\Delta t = 0$, any negative amplitude associated with the τ_1 DAS in the 0.0–0.6 eV region would be effectively compensating for the positive amplitude at short delay times associated with a sequential feature (i.e., one not truly originating from $\Delta t = 0$) described by the τ_2/τ_3 DAS in the same energy region. This is not observed in our data and so we may infer that the dynamics associated with τ_1 and τ_2/τ_3 are independent from each other. More generally, in cases where spectral features arising from different dynamical processes – with different associated ionization cross-sections – are not fully resolved from each other, we note that one must exercise far greater caution in the interpretation of DAS data in this way.
[47]C. Z. Bisgaard, O. J. Clarkin, G. Wu, A. M. D. Lee, O. Gessner, C. C. Hayden, and A. Stolow, Science **323**, 1464 (2009).
[48]Y.-I. Suzuki, T. Horio, T. Fuji, and T. Suzuki, J. Chem. Phys. **134**, 184313 (2011).